The Islamic University Journal (Series of Natural Studies and Engineering)
Vol.15, No. 2, pp 21-39, **2007**, ISSN 1726-6807, http://www.iugaza.edu.ps/ara/research/

Interpretation of Gravity Data in the Jericho Area, Dead Sea Transform

Radwan J. El-Kelani
Earth Sciences and Seismic Engineering Center (ESSEC)
An-Najah National University, P.O. Box 707, Nablus, Palestine
E-mail: radwan@najah.edu

Abstract: A detailed gravity survey was conducted in this study. More than 100 new gravity stations, with an average spacing of about 0.5 km, were measured. Qualitative interpretation of the compiled Bouguer anomaly map in the Jericho area is presented. The most prominent feature of the Bouguer anomalies is the presence of negative values mainly trending in the NNE-SSW direction. This trend reaches a horizontal gravity gradient of up to 10 mGal/km towards east. High negative anomalies of about -30 mGal are observed to occur along the eastern side caused by thick, low-density young sediments filled in the Dead Sea rift. Wavelength filtering technique was used to analyze the gravity data in order to separate the effect of regional structures from that of local geologic features. The residual anomaly map shows positive and negative anomalies that differ in their amplitudes, sizes and trends, possibly due to lateral lithological variations in the subsurface geology within the upper most part of the crust.

تفسير لمعطيات تسارعات الجاذبية في منطقة أريحا، إنهدام البحر الميت

ملخّص: تم في هذه الدراسة إجراء مسح جاذبي لمنطقة أريحا، حيث أُخِذَ قياس التسارع الأرضي النسبي على أكثر من 100 محطة موزعة بواقع مسافة 0.5 كم فيما بينها. وقد تم حساب قيم شواذ بوجير (Bouguer anomalies) من معطيات الجاذبية لإنتاج خريطة شواذ بوجير في منطقة الدراسة. وتمتاز هذه الخريطة بوجود شواذ سالبة تصل قيمتها إلى30 mGal- واقعة على إمتداد NNE-SSW من الجانب الغربي لحفرة الانهدام كما تـظهر ميـلاً حاداً يـصل الى 10 mGal/km باتجاه الشرق. وقد فُسِّرت هذه الشواذ على أنها تعكس وجود سماكات من الرسوبيات الحديثة ذات الكثافة القليلة تحت إنهدام البحر الميت. وللحصول على تفسير أوضح وأكثر تفصيلا لشواذ بوجير تم استخدام تقنية الفلترة (Wavelength filtering) بهدف فصل تأثير الشواذ الإقليمية المتسببة عن تراكيب جيولوجية عميقة وحساب ما يسمى بالشواذ المتبقية(Residual anomalies). تمتاز خريطة الشواذ المتبقية بوجود أنواع مختلفة من الشواذ تختلف بسعتها وأحجامها وامتدادها، كما تعكس القيم السالبة والموجبة لهذه الشواذ وجود تغيّر جانبي في أنواع الصخور وتوزيعها تحت السطح.

Keywords: Gravity data, Bouguer anomalies, Wavelength filtering, Residual anomalies, Jericho, Dead Sea Transform.

1. Introduction

The Dead Sea-Jordan rift separates the Arabian Plate and the Sinai Block of the African Plate (Fig.1). Transform motion, thought to have started in Miocene along the rift, is taking up the opening of the Red Sea into the zone of continental convergence in southeastern Turkey. This regional structure attracted the attention of geoscientists for many decades [e.g. 1-12]. The Jericho area is located immediately north of the Dead Sea basin, which is considered to be an active pull-apart basin: the plate transform (Figs. 1 and 2], that extends from the south along the eastern margin of the Dead Sea rift, bends to the east and dies out to the northeast.

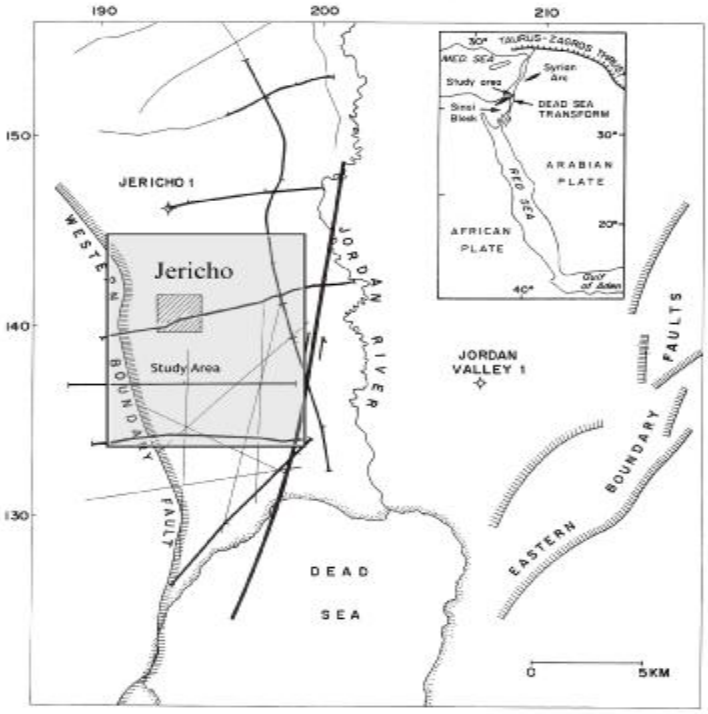

Figure 1: Location map of present study, showing the location of the study area, the seismic reflection lines [20] and the deep wells in the area. The thick line marks the location of the plate transform [19].

The next segment of the transform lies along the western side of the Dead Sea and extends obliquely across the rift in the study area [3, 13, 14, 18, 19]. Results of several seismic reflection lines in the Jericho area (Fig. 1) were described by Rotstein et. al [20]. The seismic data were used to analyze the structure of this part of the Dead Sea rift, which in this area is a zone of intense deformation.

The study area is part of the Jordan Valley, a segment of the Dead Sea Rift. It is situated between the Jordan River in the centre of the rift valley and the prominent normal fault which marks the western boundary of the rift north of the Dead Sea (Figs. 1, 2). The area was studied by Picard [15] who described the Dead Sea as a rift valley bordered by "two considerable border faults", and noted that the Western Boundary Fault is the oldest tectonic feature in the area related to this rift. He estimated the throw on the Eastern Border Fault to be several hundred meters, with most of the motion on it being pre-Late Pleistocene Lisan Formation. Rot [16] and Begin [17] studied parts of this area, but focused on the folds which are observed in the Mesozoic sequence west of the rift. They mapped, in particular, the Mar Sava and Auja anticlines and the Buqia Syncline (Fig. 2).

The present study describes and summarizes the gravity results obtained during the past few years in the Jericho area and aims at continuing geological mapping using the Bouguer anomaly map. Wavelength filtering technique was also used to analyze the available gravity data.

Surface sediments in this area are mostly horizontal, consisting mainly of coarse clastics and chalks of the Pleistocene Samra and Lisan Formation (Fig. 2), and sandstones of the Mazar Formation (Lower part of Samra Formation [21]). These beds are unconformably overlain by the Late Pleistocene Lisan Formation, known from the central Jordan Valley, and from the northern Araba Valley, south of the Dead Sea. Many wells are found in the area but most are shallow water wells (Fig. 2). Nevertheless, some of them are deep enough to penetrate prerift sediments, which appear to be quite shallow in this area (Fig.2). Jericho 1 is the only deep well in the area and is located on pre-rift Senonian chert. Jordan Valley 1, which is the only drill hole in the eastern side of the rift, penetrated 276 m of Neogene to Pleistocene clastic rift sediments overlying pre-rift Lower Eocene beds. Thus, a deep basin does not exist in the Jericho area and the transform is characterized by strike-slip motion [22].

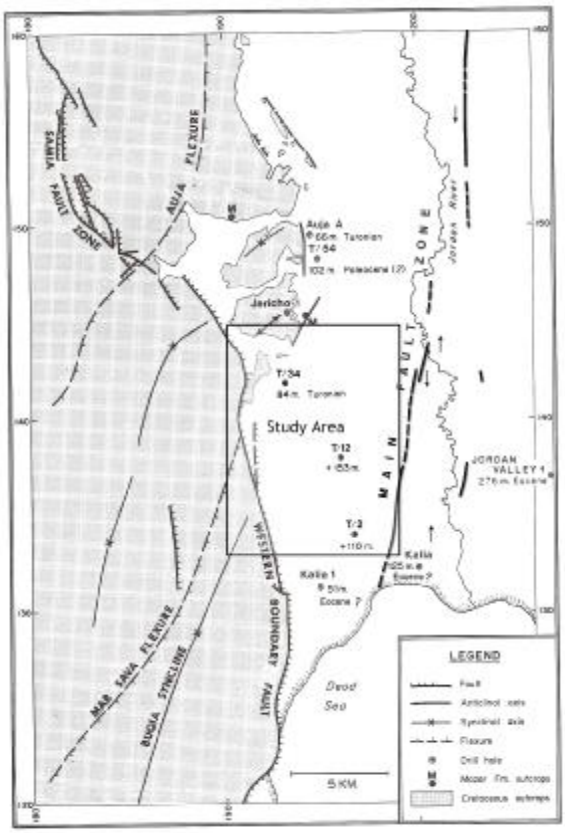

Figure 2: Simplified geological map of the study area. Also shown are wells in which pre-rift Upper Mesozoic and Tertiary sediments were found; numbers indicate depth to pre-rift sediments, and their ages appear when known. The transform is recognized by the terrace (bold dashed lines) which it forms in the white chalk of the Pleistocene Lisan Formation; it is marked by arrows.

The Dead Sea Transform in the study area is known to be seismically active. The last known strong earthquake in the area was the Jericho event (M=6.25) in 1927 [18]. Strong earthquakes in this area have a repeat time of several hundred years [19, 23]. Nevertheless, the seismic activity in the area is presently quiet high, possibly because enough amounts of strain have accumulated since the last strong earthquake [24, 25].

2. Gravity Measurements and Analyses

2.1 New Gravity Data

To improve coverage of gravity data in the Jericho area, measurements were made during February-April 1999 at 102 new gravity station with an average spacing of about 0.5 km (see Fig. 3 and Table 1). Field measurements were carried out using the Lacoste and Romberg gravimeter Model G833. Base station was occupied at the beginning and end of each working day. During the field survey, the daily drift was usually less than 1 mGal. It is estimated that the error in the Bouguer gravity values is approximately ± 0.2 mGal. All the gravity measurements, including the new and the previous data, were linked to the reference base gravity station *Beit Ha'arava* (g = 979511.3, X=1197387, Y= 1134118, Z= -343.76 m).

The Geographic Positioning System (GPS) was used for geodetic measurements. The gravity stations were positioned using new GPS ProMARK X-CP instruments manufactured by the Magellan Systems Corporation. These instruments were used in the stationary differential 3-dimensional mode. Pseudo-range and carrier phase satellite data, collected on the control and remote stations at one-second intervals, were processed using the MSTAR differential post-processing system. The elevation accuracy, estimated on a number of repeated measurements and known benchmarks, is better than 20 cm. This accuracy can be obtained by using a multipath-resistant antenna for the following conditions: remote control station distance should be less than 10 km and occupation time about ten minutes. The raw gravity data were reduced using the standard procedures [26]. The latitude correction and the theoretical values of gravity were calculated from the International Gravity Formula 1967 [26] which gives the value of g at any point on this spheroid as:

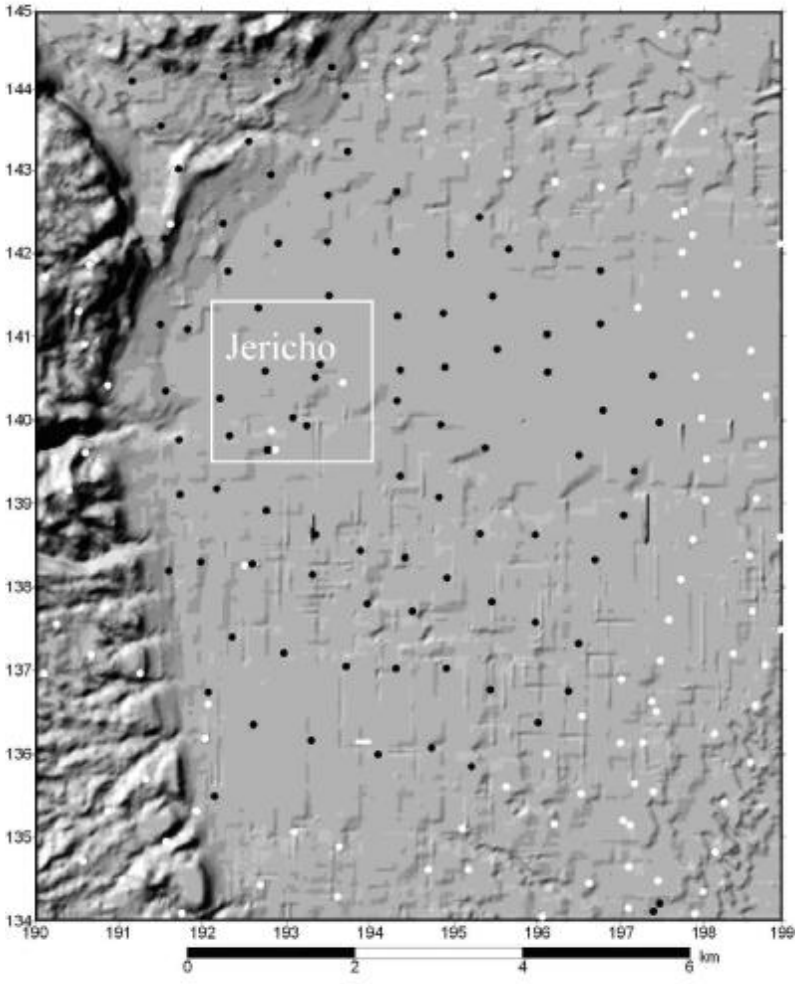

Figure 3: Gravity coverage map of the Jericho area; black dots donate the new gravity stations; white dots are the old stations.

$$g = g_0(1 + a \sin^2 f + ß \sin^2 2f) \quad (1)$$

Where:

g_0 = 978.0318 Gal (equatorial gravity)

a = 0.0053024

$ß$ = - 0.0000058

f = Latitude

Table 1: Summary of the important data of the new gravity points in the study area.

Station No.	X (m)	Y (m)	Observed Gravity	Elevation (m)	Free-air	Bouguer	Terrain reduction
1139	1192775	1139643	979512.1	-239.15	-32.51	-5.76	0.85
1140	1193075	1140032	979513.8	-246.85	-33.93	-6.32	0.72
1141	1193344	1140512	979514.9	-249.26	-33.5	-5.61	0.6
1142	1193384	1141081	979515.8	-249.86	-33.54	-5.59	0.59
1143	1193508	1141494	979516.2	-249.56	-33.04	-5.12	0.58
1144	1193488	1142139	979517	-245.46	-31.73	-4.27	0.62
1145	1193498	1142701	979516.7	-235.46	-28.96	-2.62	0.66
1146	1193734	1143222	979515.7	-229.16	-28.7	-3.06	0.72
1147	1193705	1143916	979515.8	-217.76	-25.14	-0.78	0.9
1148	1193540	1144287	979513.6	-198.36	-22.05	0.14	0.91
1149	1193935	1145977	979508.8	-177.16	-21.06	-1.24	0.78
1150	1192893	1144107	979512.3	-184.23	-19	1.61	0.93
1151	1192254	1144164	979509.8	-170.06	-17.18	1.84	1.06
1152	1191572	1144261	979504.9	-142.26	-13.45	2.47	1.4
1153	1191161	1144111	979505.6	-147.06	-14.23	2.23	1.45
1154	1191504	1143538	979508.9	-167.52	-16.6	2.14	1.29
1155	1191709	1143012	979509.8	-176.56	-18.43	1.32	1.88
1156	1192247	1142354	979517.4	-218.16	-22.91	1.49	0.88
1157	1192819	1142938	979514.8	-209.6	-22.86	0.59	0.86
1158	1192547	1143339	979511.4	-187.56	-20.2	0.78	1.19
1159	1192301	1141783	979517.2	-225.96	-24.79	0.49	0.86
1160	1192774	1139647	979512.1	-239.02	-32.38	-5.64	0.85
1161	1192068	1136741	979508.9	-229.06	-30.42	-4.8	1
1162	1192350	1137403	979510.4	-242.61	-33.72	-6.57	0.96
1163	1192969	1137211	979510.8	-252.36	-36.4	-8.16	0.8
1164	1193711	1137054	979511.9	-261.26	-37.97	-8.74	0.68
1165	1194308	1137028	979512.6	-268.96	-39.69	-9.6	0.61
1166	1194912	1137027	979513.3	-277.92	-41.75	-10.66	0.6
1167	1195436	1136769	979513.4	-288.26	-44.22	-11.97	0.5
1168	1196004	1136377	979513.1	-298.26	-47.58	-14.21	0.51
1169	1196367	1136756	979512.7	-300.96	-48.84	-15.17	0.5
1170	1196491	1137325	979513.6	-302.06	-48.93	-15.14	0.45
1171	1195974	1137579	979513.6	-293.28	-46.17	-13.36	0.43
1172	1195452	1137827	979514.4	-284.96	-42.8	-10.92	0.43
1173	1194922	1138110	979514.6	-275.98	-40.66	-9.78	0.48
1174	1194420	1138352	979514.6	-269.67	-38.72	-8.55	0.56
1175	1193882	1138437	979513.9	-262.96	-37.32	-7.9	0.63
1176	1193350	1138625	979513.5	-256.76	-35.77	-7.04	0.93

1177	1192758	1138922	979512.4	-245.53	-33.4	-5.93	0.85
1178	1192773	1139647	979512.3	-239.1	-32.32	-5.57	0.85
1179	1192597	1138278	979510.8	-241.06	-33.67	-6.7	0.9
1180	1193311	1138153	979512.6	-256.82	-36.7	-7.97	0.71
1181	1193968	1137802	979515.1	-273.26	-38.5	-7.93	0.6
1182	1194508	1137710	979513.6	-271.45	-39.52	-9.15	0.62
1183	1192068	1136741	979508.8	-229.1	-30.58	-4.95	1
1184	1192777	1139646	979512.1	-239.12	-32.4	-5.65	0.85
1185	1194359	1140604	979516	-264.49	-37.1	-7.51	0.48
1186	1194892	1140634	979516.9	-273.16	-38.92	-8.36	0.44
1187	1195514	1140850	979517.1	-279.96	-40.86	-9.54	0.41
1188	1196115	1141028	979516.8	-286.67	-43.87	-11.8	0.38
1189	1196751	1141153	979516.9	-298.06	-47.26	-13.91	0.36
1190	1196751	1141790	979517.1	-295.84	-46.43	-13.34	0.37
1191	1196221	1141989	979517.3	-284.36	-42.7	-10.89	0.4
1192	1195660	1142048	979517.5	-275.49	-40.49	-9.67	0.41
1193	1195467	1141485	979516.9	-275.06	-40.18	-9.41	0.44
1194	1195305	1142432	979517.3	-266.96	-38.03	-8.17	0.45
1195	1194877	1141284	979517.1	-270.16	-38.51	-8.28	0.45
1196	1194330	1141252	979516.9	-263.76	-36.7	-7.2	0.49
1197	1194311	1142026	979516.9	-256.26	-35.1	-6.43	0.51
1198	1194959	1141985	979517.3	-265.56	-36.88	-7.17	0.45
1199	1194319	1142734	979516	-246.06	-32.87	-5.35	0.6
1200	1192906	1142118	979518.6	-239.34	-28.22	-1.44	0.7
1201	1192666	1141344	979515.3	-233.06	-28.86	-2.79	0.73
1202	1192745	1140591	979514.2	-239.03	-31.09	-4.35	0.76
1203	1192207	1140261	979512.5	-229.06	-29.7	-4.08	1.08
1204	1191561	1140350	979512.3	-209.76	-24.01	-0.54	1.59
1205	1191497	1141148	979514.6	-205.86	-21.22	1.81	1.87
1206	1191555	1142175	979502.8	-149.3	-16.28	0.42	1.71
1207	1191818	1141089	979515.9	-221.46	-24.62	0.16	1.34
1208	1192776	1139648	979512.1	-239.01	-32.44	-5.7	0.85
1209	1200564	1134260	979501.5	-377.58	-82.12	-39.88	0.39
1210	1201050	1134291	979500.4	-375.62	-82.59	-40.56	0.43
1211	1201759	1134338	979502.3	-382.24	-82.73	-39.97	0.46
1212	1200683	1138678	979503.3	-350.9	-75.01	-35.75	0.52
1213	1201842	1138357	979509.6	-384.5	-79.05	-36.03	0.53
1215	1201437	1137320	979507.8	-382.05	-79.51	-36.77	0.46
1216	1201167	1138507	979504.4	-359.78	-76.63	-36.38	0.61
1217	1201422	1142350	979513.8	-379.02	-76.17	-33.77	0.48
1218	1200943	1142147	979513.1	-375.19	-75.65	-33.68	0.47
1219	1200490	1142067	979512.7	-368.23	-73.88	-32.69	0.42

1220	1200017	1142269	979514	-361.93	-70.63	-30.14	0.46
1221	1192776	1139648	979511.9	-239.01	-32.57	-5.83	0.85
1222	1194325	1140231	979515.4	-264.26	-37.63	-8.07	0.5
1223	1194844	1139949	979515.5	-271.43	-39.04	-8.68	0.49
1224	1195380	1139669	979515.8	-280.54	-41.56	-10.17	0.43
1226	1196496	1139579	979515.1	-296.44	-47.09	-13.93	0.36
1227	1197156	1139392	979514.4	-308.49	-51.6	-17.09	0.36
1228	1197456	1139974	979514.3	-311.7	-52.72	-17.85	0.35
1229	1197377	1140533	979514.9	-310.33	-52.36	-17.64	0.36
1230	1196780	1140119	979515.6	-300.57	-48.71	-15.08	0.37
1231	1196118	1140576	979516.2	-288.57	-44.39	-12.1	0.38
1232	1197028	1138862	979514.3	-308.22	-50.93	-16.44	0.39
1233	1196689	1138329	979513.4	-301.97	-49.9	-16.12	0.4
1234	1195973	1138627	979515	-292.93	-45.41	-12.64	0.4
1235	1195311	1138641	979514.6	-280.21	-41.94	-10.59	0.49
1236	1194824	1139078	979516.4	-278.42	-40.28	-9.13	0.44
1237	1194359	1139331	979515.4	-269.43	-38.49	-8.35	0.5
1238	1192322	1139817	979512.6	-232.18	-29.78	-3.81	1.03
1239	1191720	1139762	979511.6	-217.5	-26.34	-2.01	1.51
1240	1191727	1139108	979511.1	-218.27	-27.08	-2.66	1.3
1241	1192775	1139648	979512.8	-238.99	-31.75	-5.02	0.85
1268	1198547	1156556	979523.1	-304.04	-53.93	-19.92	0.42

The gravity data were reduced using a rock density 2670 kg/m^3. The terrain correction was calculated using relief in the form of a digital terrain model with a 25 meter grid, adopted from the Digital Terrain Model (DTM) compiled by Hall [27].

2.2 Qualitative Interpretation of Gravity Data

The gravitational field of the Earth varies from the equator to the poles due to the flattening of the earth as well as its rotation. Therefore, the observed gravity differences, before being exploited, must be corrected to compensate for the above mentioned facts and all those influencing values apart from the distribution of density of the subsurface matter. After performing the corrections, the end product is usually a contoured map of the Bouguer gravity anomaly.

Qualitative interpretation of a Bouguer anomaly map gives valuable information about anomalous objects and subsurface structures in terms of their location, size, shape and other characteristics. The nature of anomalous gravitational fields depends on the following main aspects of crustal structures [28]:

1. Variation in the general thickness of the crust (i.e the relief of the Moho discontinuity) and density differences of the subcrustal matter;
2. The existence of large tectonic disturbances and the splitting of the crust into separate blocks;
3. The variation in the thicknesses, petrographic compositions and structures of the different layers of the crust (anomalous geologic features).

The Bouguer anomalies at the new stations, together with those previously measured (Fig. 3), were used to compile a Bouguer anomaly map of the Jericho area (Fig. 4). The compiled Bouguer anomaly map displays a strong regional gravity anomalies striking mainly NNE-SSW, associated with deep-seated lateral density changes. These changes might be related to a difference existing in the upper crustal lithology. For example, under the eastern side of the study area rocks are very thick, low-density young sediments. Also, local, short-wavelength, positive and negative gravity anomalies are superimposed on the main gravity gradient associated with near-surface density variations. However, the detailed Bouguer anomaly map of the study area (Fig. 4) shows different anomalies that vary in size, wavelength, amplitude and direction. The following is a brief description of both the positive and negative anomalies:

(i) At the western side of the map, there exist positive and negative anomalies. Their amplitudes are between 2 and -6 mGal of an average wavelength (width) of about 2.4 km.

(ii) At the eastern side, the map is characterized by negative Bouguer values which increase to a maximum value of about -30 mGal.

(iii) Due to the Dead Sea rifting, the main regional gravity anomalies trend decreases significantly eastward (see also Fig. 5) with a steep gradient of up to 10 mGal/km.

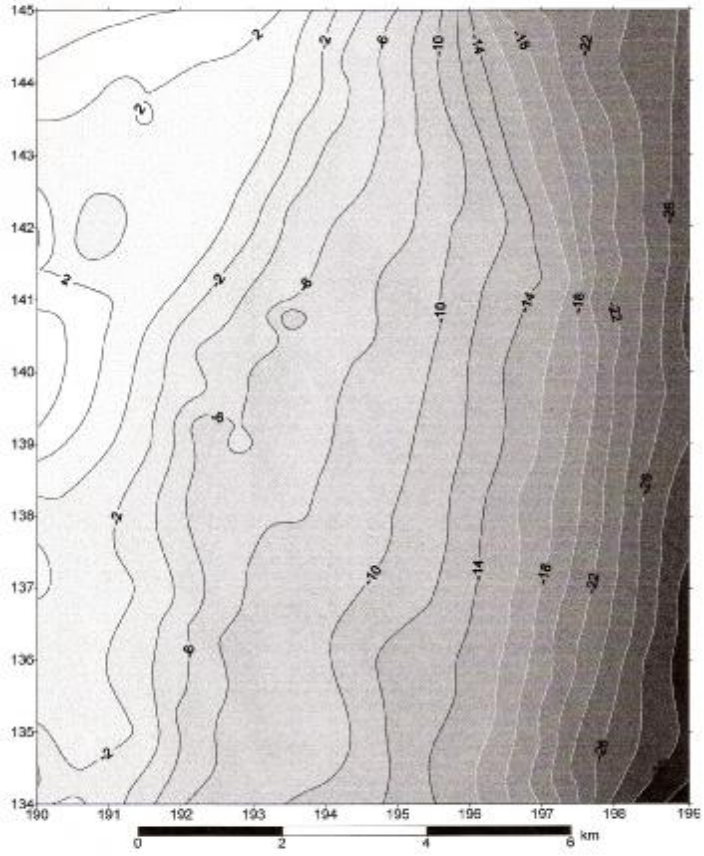

Figure 4: Bouguer anomaly map of the Jericho area (contour interval 2 mGal).

2.3 Filtered Gravity Maps

It is usually of great value to separate an observed gravity or magnetic field into regional and residual parts. This enables anomalies, associated with various depths below the surface, to be identified in a qualitative way. It helps also to distinguish between large and small structures in a given study area. Several methods, including numerical and graphical treatments, have been recommended for separating the regional from the Bouguer anomalies and obtaining the residual fields [29-35]. The technique used here in the analysis of the gravity data is the wavelength filtering determination of Degro [35]. The filtering operations are done in the frequency domain by multiplication of the transfer function $\Psi(k_x, k_y)$ with the Fourier transform $F(k_x, k_y)$ of a given data $f(x,y)$. The final results are transformed back into the space domain by inverse Fourier transform [34-36]:

$$\Phi(x,y) = F^{-1}(\Psi(k_x, k_y) * F(k_x, k_y)) (x,y) \quad (2)$$

In the separation of the regional and residual fields, a certain cut-off wavelength (l_c) is identified. Anomalies for which $l \leq l_c$ are suppressed or isolated are referred to as residuals. The choice of a cut-off wavelength must be related to the depth of the disturbing body. The approximate relationship between the maximum depth z_S of a causative body and the half width $b_{1/2}$ is given by Jung [37] as:

$$z_S \leq 0.5\, b_{1/2} \text{ (2-dimensional)} \quad (3)$$

$$z_S \leq 0.652\, b_{1/2} \text{ (3-dimensional)} \quad (4)$$

An approximate formula for the selection of the boundary wavelength is given as:

$$l_c \geq 3\, z_S \text{ (3-dimensional)} \quad (5)$$

This can also be obtained from the anomaly map as:

$$l_c = 2\, b_{1/2} \text{ (3-dimensional)} \quad (6)$$

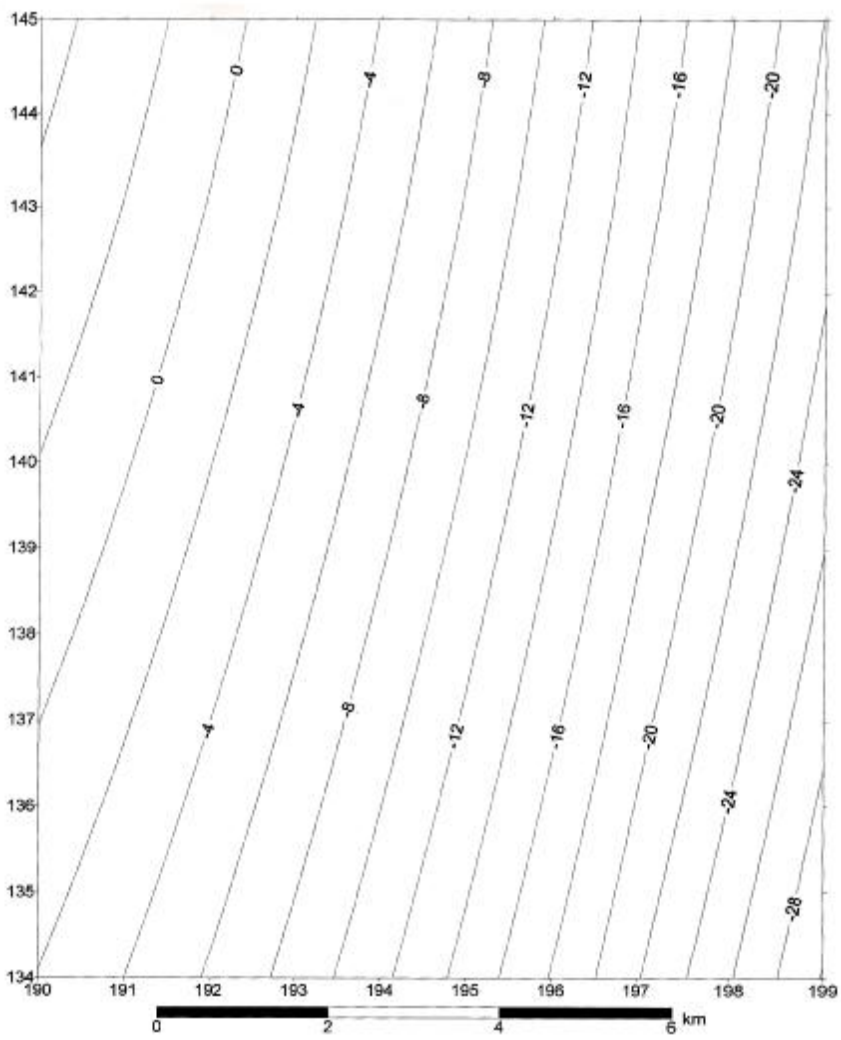

Figure 5: Regional anomaly map of Jericho area (contour interval 2 mGal).

The regional and the residual anomaly maps, obtained after wavelength filtering, are shown in Fig. 5 and Fig. 6. A total 210 gravity stations were used over an area of about 120 km^2. One of the main objectives of the wavelength filtering was an attempt to relate the anomalies to their depth of origin and to identify persistent trends at selected wavelengths of cut-off.

The estimations of the depth of origins were made by using the 3-dimensional approximation equations given in this section. The wavelength of cut-off (l_c), selected in this study, is 2.4 km as deduced from the Bouguer anomaly map (Fig. 4, see also the relationship Nr. 6).

The regional anomaly map shown in Fig. 5 gives the case with a cut-off wavelength of 2.4 km. The main feature of this map is the NNE-SSW trend that the gravity anomalies decrease towards the eastern side of the study area. This is probably caused by deep seated basins of light sediments. At this wavelength, the residual anomalies (Fig. 6) are associated with small features and the major regional trends become less clearly defined. They are characterized by different amplitudes and widths range from –3 to 2 mGal and of about 0.8 to 3.1 km respectively that could be related to lateral lithological variations within the subsurface geology in the upper most part of the crust. On the other hand, the distribution of the residual anomalies could represent an existing of subsurface synclines and anticlines beneath the study area (see Fig. 2).

3. Results and Discussion

In the present study, the results obtained from the analysis and interpretation of the gravity data in the Jericho area were constrained by previous geophysical and geological studies. Attempts are made to evaluate the type of agreement between the gravity anomalies and the known geology. It is suggested, geologically, that the causative sources of the positive and negative gravity anomalies (Figs. 4 and 6) are subsurface geological structures associated with the origin of the Dead Sea rift. Such that under the western side of the study area, the local gravity anomalies (Fig. 6) are assumed to be related to near surface density variations occurred in the upper crustal lithology (Fig. 2), while under the eastern side, high negative anomalies (Fig. 4) are caused by thick, low density young sediments filled in the Dead Sea rift [8, 12, 20].

potential field is much smoother for the northeastern and southeastern. The complex parts are referred to near-surface wide zone of intense deformation in the sedimentary cover and geological features [15, 20] associated with the tectonic activities and evolution of the Western Boundary Fault and the main fault zone (Figs. 1 and 2).

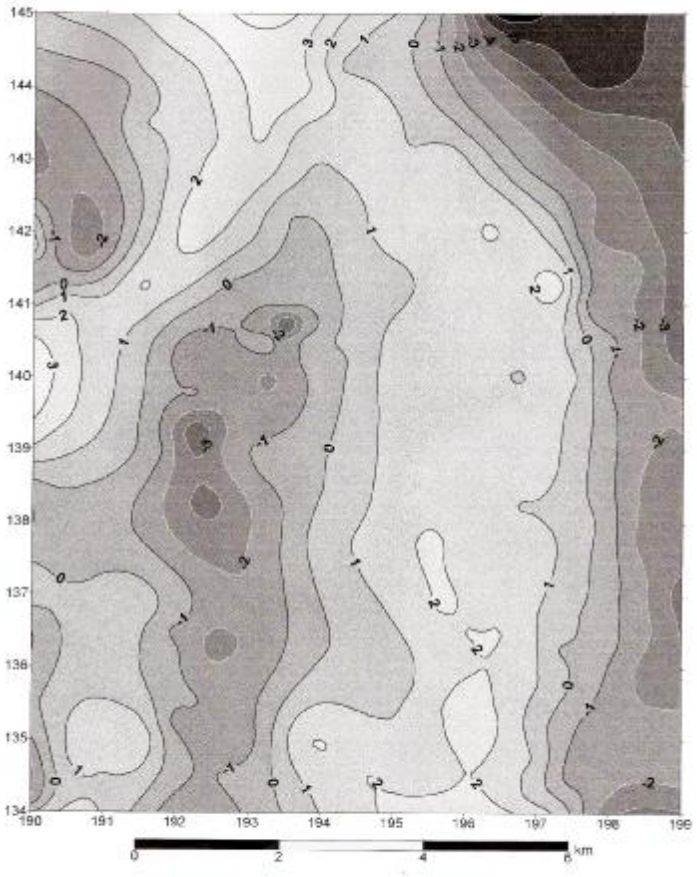

Figure 6: Residual anomaly map of Jericho area (contour interval 1 mGal).

The regional anomalies, mainly trending in the NNE-SSW direction (Figs. 4 and 5), display rapid changes in the gravity values eastward with a horizontal gravity gradient of up to 10 mGal/km. This could be related to the crustal shifting towards the northeast during the development of the transform plate boundary between the Arabian Plate and the Sinai Block of the African Plate (Fig.1). The nature of the gravitational field is complex for the northwestern, southwestern and central parts (Figs. 4 and 6), while the

For the purpose of detailed qualitative interpretation of the Bouguer anomalies, wavelength filtering was performed. The filtered anomaly map (Fig. 6) shows the causative sources of such anomalies at selected wavelength of cut-off (l_c), where the origin depths of the anomalies can be estimated by using the 3-dimensional approximation equations given in section (2.3). The estimated depth of the causative sources of the local anomalies (Fig. 6) ranges from intermediate (about 1 km) to shallow (less than 0.3 km), where deep basins have not been reported in the Jericho area [22]. On the other hand, the alternating positive and negative anomalies (Fig. 6) tend to agree with the surface geology and structural features in the western part of the study area (Fig. 2).

In the eastern part of the study area, a good fitting can be observed between the present gravity interpretation and the results of the seismic reflection data [20], where gravity gradient evidence of near-surface thrust deduced from the filtered Bouguer anomaly map (Fig. 6), at 2.4 km cut-off wavelength, indicate that the main fault zone (Figs. 1 and 2) dips to the west, a way from the rift, suggesting that although most of the motion is of strike-slip nature, a reverse-motion component is also present. Furthermore, reversed faulting is computed by number of earthquake source mechanisms from the study area, demonstrating that compression, associated with thrusting, is still active [20].

The analysis and interpretation of the gravity data reveal some aspects about the structure of the Jericho area which are useful for supplementing other data in the geological synthesis. Although there is lack of uniform ground coverage of the gravity stations, the data were good enough for delineating shallow structures and fitting the basic information supplied by the previous geophysical investigations, especially the seismic results, as well as from geological knowledge.

Acknowledgements

Part of the gravity data in the investigated area were measured by the author during his work at the Earth Sciences and Seismic Engineering Center (ESSEC) at An-Najah National University, Nablus, Palestine. He is very grateful to the ESSEC staff for facilitating the necessary arrangements during the survey. I am deeply grateful to the USAID for financing the field work.

References

[1] Quennell A.M., 1959- *Tectonic of the Dead Sea Transform*. Cong. Geol. Int. Maxico, Vol. 22, p: 385-405.

[2] Ginzburg A., Makris J., Fuchs K., Prodehl C., 1981- *The structure of the crust and upper mantle in the Dead Sea Transform*. Tectonophysics, Vol. 80, p: 109-119.

[3] Garfunkel Z., 1981- *Internal structure of the Dead Sea leaky transform (rift) in relation to plate kinematics*. Tectonophysics, Vol. 80**,** p: 81-108.

[4] El-Isa Z.H., and Kharabsheh A.R., 1982- *Magnetic and gravity studies of the northern Dead Sea Rift*. In Abed and Khaled (eds.), Proceedings of the 1st Jordan Geological Conference, Amman, p: 483-501.

[5] Folkman Y., 1981- *Structural features in the Dead Sea-Jordan Rift zone, interpreted from combined magnetic-gravity study*. Tectonophysics, Vol. 80, p: 135-146.

[6] Quennell A.M. 1983- *Evolution of the Dead Sea Transform*. A review in Abed and Khaled (eds.), Proc. 1st Jord. Geol. Conf., Amman, p: 460-482.

[7] El-Isa Z., Mechie J., Prodehl C., Makris J., Rihm R., 1987- A crustal structure study of Jordan derived from seismic refraction data. Tectonophysics, Vol. 138, p: 235-253.

[8] Hassouneh M., 2003- *Interpretation of potential fields by modern data processing and 3-dimensional gravity modelling of the Dead Sea pull-apart basin/ Jordan Rift Valley (JRV)*. Dissertation, Würzburg University, p: 110.

[9] Haberland Ch., Agnon A., El-Kelani R., Maercklin N., Qabbani I., Rümpker G., Ryberg T., Scherbaum F., Weber M., 2003- *Modeling of seismic guided waves at the Dead Sea Transform*. J. Geophys. Res., Vol.108, No. B7/2342, p: 1-11.

[10] Ruepker G., Ryberg T., Bock G., Weber M., Abu-Ayyash K., Ben-Avraham Z., El-Kelani R., Garfunkel Z., Haberland C., Hofstetter A., Kind R., Mechie J., Mohsen A., Qabbani I., Wylegalla K., 2003- *Boundary-layer mantle flow under the Dead Sea Transform fault from seismic anisotropy*. Nature, Vol. 425, p: 497-501.

[11] Weber M., Abu-Ayyash K., Abueladas A., Agnon A., Al-Amoush H., Babeyko A., Bartov Y., Baumann M., Ben-Avraham Z., Bock G., Bribach J., El-Kelani R., Förster A., Förster H-J., Frieslander U., Garfunkel Z., Grunewald S., Götze H-J., Haak V., Haberland Ch., Hassouneh M., Helwig S., Hofstetter A., Jäckel K-H., Kesten D., Kind R., Maercklin N., Mechie J., Mohsen A., Neubauer F.M., Oberhänsli

R., Qabbani I., Ritter O., Rümpker G., Rybakov M., Ryberg T., Scherbaum F., Schmidt J., Schulze A., Sobolev S., Stiller M., Thoss H., Weckmann U., Wylegalla K., 2004- *The crustal structure of the Dead Sea Transform.* Geophys. J. Int., Vol.156, p: 655-681.

[12] El-Kelani R., 2006- *3-dimentional gravity model of the southern Jordan Dead Sea Transform.* An-Najah University Journal for Research-A (Natural Sciences), Vol. 19, p: 185-208.

[13] Freund R., Garfunkel Z., Zak I., Goldberg M., Weissbrod T., and Derin B., 1970- *The shear along the Dead Sea Rift*. Philos. Trans. R. Soc. London, Vol. 267, Ser. A, p:107-130.

[14] Aydin A., and Nur, A., 1982- *Evolution of pull-apart basins and their scale independence*. Tectonics, Vol. 1 p: 91-105.

[15] Picard L., 1931- *Geological researches in the Judean Desert*. Geological Survey of Israel (GSI), p:108.

[16] Rot I., 1970- *The Geological map of Israel*. Geological Surv. Isr (GSI), Wadi el Qilt, 1:50000.

[17] Begin Z.B., 1975a- *The geology of the Jericho sheet.* Geological Surv. Isr. Bull. 67, p: 1-35.

[18] Ben-Menahem A., Nur A., and Vered M., 1976- *Tectonics, seismicity and structure of the Afro-Eurasian Junction- the breaking of an incoherent plate*. Phys. Earth Planet. Inter., Vol. 12, p: 1-50.

[19] Reches Z., and Hoexter D.F., 1981- *Holocene seismic and tectonic activity in the Dead Sea area*. Tectonophysics, Vol. 80, p: 235-254.

[20] Rotstein Y., Bartov Y., and Hofstetter A., 1991- *Active compressional tectonics in the Jericho area, Dead Sea Rift.* Tectonophysics, Vol. 198, p: 239-259.

[21] Begin Z.B., 1975b- *Paleocurrents in the Plio-Pleistocene Samra Formation (Jericho region) and their tectonic implication*. Sediment. Geol., Vol. 14 p: 191-218.

[22] Kashai E.I., and Croker, P.F., 1987- *Structural geometry and evolution of the Dead Sea-Jirdan Rift system as deduced from new subsurface data*. Tectonophysics, Vol. 141 p: 33-60.

[23] Rotstein Y., 1987- *Gaussian probability estimates of large earthquake occurrence in the Jordan valley, Dead Sea Rift.* Tectonophysics, Vol.141, p: 95-105.

[24] Al-Dabbeek J., and El-Kelani R., 2004- *Local site effect in Palestinian cities: a preliminary study based on Nablus earthquake of July 11, 1927 and the earthquake of February 11, 2004.* The 1st Conference of Applied Geophysics for Engineering, 13-15 October, Messina, Italy.

[25] Al-Dabbeek J., and El-Kelani R., 2005- *Dead Sea Earthquake of February 2004, ML 5.2: post earthquake damage assessment*. The International Earthquake Conference (TINEE), 21-24 November, Dead Sea, Jordan.

[26] Telford W., Geldart L., Sheriff R., and Keys A., 1976- **Applied Geophysics**. New York, Cambridge, p: 14-30.

[27] Hall J.K., 1993- *The GSI Digital Terrain Model (DTM) completed*. In: Bogoch R., and Eshet Y., (ed), GSI Current Research, p: 47-50.

[28] Sazhina N., and Grushinsky N., 1971- **Gravity Prospecting**. Moscow, Mir Publisher, p: 63-71.

[29] Griffin W.R., 1949- *Residual gravity in theory and practice*. Geophysics, Vol. 14, p: 39-56.

[30] Elkins T.A., 1951- The *Second Derivative Method of gravity interpretation*. Geophysics, Vol. 16, p: 29-50.

[31] Rosenbach O., 1953- *A Contribution to the Computation of the Second Derivative from Gravity Data*. Geophysics, Vol. 18, p: 894-912.

[32] Nettleton L.L., 1954- *Regionals, residuals and structures*. Geophysics, Vol. 19, p: 1-22.

[33] Henderson R.G., and Zietz I., 1949- *The Computation of Second Vertical Derivatives of geomagnetic fields*. Geophysics, Vol. 14, p: 508-516.

[34] Black D.I., and Scollar I., 1969- *Spatial Filtering in Wave-Vector Domain*. Geophysics, Vol. 34, p: 916-923.

[35] Degro T., 1986- *Zur Interpretation gravimetrisscher und magnetischer Feldgroessen mit Hilfe von Uebertragungsfunktionen*. Dissertation, Clausthal Technical University, Germany, p:18-96.

[36] Zurflueh E., 1967- *Application of two-dimensional Linear Wavelength Filtering*. Geophysics, Vol. 32, p: 1015-1035.

[37] Jung K., 1961- **Schwerkraftverfahren in der angewandten Geophysik**. Akademische Verlagsgesellschaft Gees and Portig K. G., Leipzig, p: 16-19.

[38] Geophysical Institute of Israel (GII) 1999- *Gravity and magnetic data from Israel and adjacent Areas*. Job No. 840/63/99, p: 1-11.